ACS OMEGA

Article

Cite This: ACS Omega 2019, 4, 6903−6913

http://pubs.acs.org/journal/acsodf

Effect of Synthesis Techniques on the Optical Properties of Ho^{3+}/Yb^{3+} Co-doped YVO_4 Phosphor: A Comparative Study

Abhishek Dwivedi,[†] Ekta Rai,[‡] Devendra Kumar,*[,†] and Shyam B. Rai*[,‡]

[†]Department of Ceramic Engineering, IIT (BHU), 221005 Varanasi, India

[‡]Department of Physics, BHU, 221005 Varanasi, India

ABSTRACT: The Ho^{3+}/Yb^{3+}-codoped YVO_4 phosphors have been synthesized by three different techniques (viz., solution combustion, sol−gel, and solid-state reaction techniques). X-ray diffraction patterns confirm the formation of a pure phase in the samples synthesized by all of the three methods; however, the average crystallite sizes in the three cases are different. The crystallite size increases if they are heated to higher temperature. The particle sizes are measured by scanning electron microscopy, which shows an increase in particle size with increasing the calcination temperature. The vibrational behavior of all of the three synthesized phosphor samples is studied by the Fourier transform infrared (FTIR) technique. The UV−vis absorption measurements give a large number of bands in all of the three samples prepared by three different methods. The upconversion (UC) emissions in all three samples have been monitored using a 980 nm diode laser. It gives an intense red emission in all of the three samples. Upconversion emission intensity is more prominent in the phosphor sample synthesized by the sol−gel technique and heated at 1473 K. The enhancement in UC emission intensity is well understood by the shape and size of the particles and also confirmed by the FTIR and UV−vis measurements. It is interesting to note that whereas UC measurements give red and weak green emissions, downshifting (DS) measurements show intense green, weak red, and broad blue emissions on UV excitation (323 nm). The DS behavior shows the same characteristics of the enhancement in overall emission. Overall, the phosphor sample synthesized by the sol−gel method gives better results in upconversion and downshifting behaviors when heated at 1473 K.

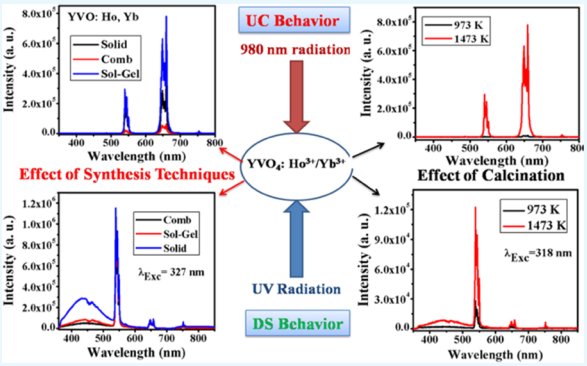

1. INTRODUCTION

Rare-earth-doped materials have wide applications in different fields such as in the development of new lasers, light-emitting diodes, display devices, plasma panels, solar panels, for bioimaging, as a sensor, etc.[1−8] The upconversion (UC) emission from rare-earth-doped materials on near-infrared (NIR) excitation is often used in the field of life sciences to get valuable information as the biomaterials do not degrade by weak NIR radiation. Some of these rare-earth-doped materials show dual-mode emissions in which both upconversion (UC) and downshifting (DS) emissions are observed.[9,10] Rare earth ions doped in these act as an activator, which shows upconversion emission on NIR pumping and downconversion on UV/visible pumping. The hosts that have been used are generally glass, polymer, inorganic or organic phosphor, composites, etc. In this work, we have used an inorganic material as a host. The host materials and their preparation method, purity, and quality play a very important role in luminescence. The host material may be a self-activated host or non-self-activated host. The self-activated host materials absorb the incident UV light and give broadband emission in the UV−visible region, which sensitizes not only the rare earth (activator) but also sometimes the other activators (if used) doped in it. YVO_4 is such a self-activated host that gives intense broad emission in the 350−550 nm region on UV excitation. The rare earth ion (Ho^{3+}) doped in YVO_4 absorbs this radiation and gives its own intense emission in the green region. The phonon frequency of this host is low (≈800 cm^{-1}), which is suitable for better UC emission behavior. The UC emission intensity may be enhanced significantly by codoping of the Yb^{3+} ion with Ho^{3+} in YVO_4 phosphor.[10]

As mentioned above, the optical emission behavior of an activator in a host strongly depends on its synthesis procedure. It is well known that the shape and size of the particles can be controlled by using different techniques.[11,12] It is also reported that on heating/calcination at higher temperatures, the average particle size of the synthesized phosphors increases,[13,14] which shows an interesting effect on the optical emission behaviors, viz., UC as well as downshifting. Silver et al.[15] have reported that the increase in particle size increases the UC emission efficiency. Wang et al.[16] have also suggested that the luminescence property enhances with the increase in the particle size.

Received: December 22, 2018
Accepted: April 4, 2019
Published: April 16, 2019

DOI: 10.1021/acsomega.8b03606
ACS Omega 2019, 4, 6903−6913

There are several methods for the synthesis of rare-earth-doped phosphor materials. In the present work, three different methods (viz., solution combustion, sol−gel, and solid-state reaction methods) have been used for the synthesis of Ho^{3+}/Yb^{3+}-codoped YVO_4 phosphor. The samples are synthesized by combustion and sol−gel methods. Parts of these samples are heated at 973 and 1473 K. At the next step, Ho^{3+}/Yb^{3+}-codoped YVO_4 phosphor is prepared at 1473 K using the solid-state reaction method. The optical as well as the structural properties of all of the samples are compared. It is found that the phosphor sample synthesized by the sol−gel technique shows better optical behavior than the phosphor samples synthesized by combustion or solid-state reaction methods. Such types of comparative studies of both structural and optical properties in phosphors synthesized by different techniques are rarely reported to the best of our knowledge.

In the present work, an enhancement in overall emission (UC and DS) has been observed and it is analyzed using X-ray diffraction (XRD), scanning electron microscopy (SEM), and Fourier transform infrared (FTIR) and UV−vis−NIR measurements. The intense red emission observed in the upconversion process is applicable in bioimaging. In brief, the phosphor sample synthesized by the sol−gel technique shows better optical properties than those of the samples prepared by the other two methods.

2. RESULTS AND DISCUSSION

2.1. Structural Morphology. Figure 1a shows the X-ray diffraction pattern of the YVO_4:Ho^{3+},Yb^{3+} phosphor samples

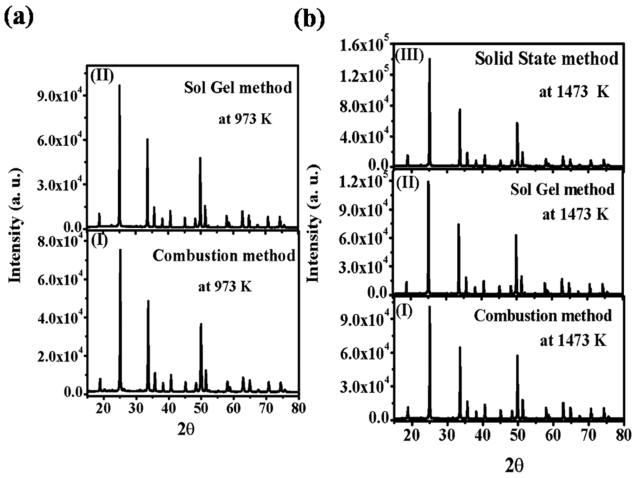

Figure 1. (a) X-ray diffraction patterns of YVO_4:Ho^{3+},Yb^{3+} synthesized by (I) combustion and (II) sol−gel methods at 973 K; (b) XRD patterns of phosphors synthesized by (I) combustion, (II) sol−gel, and (III) solid-state reaction methods at 1473 K.

synthesized by two different methods (i.e., combustion and sol−gel) and heated at 973 K. The XRD patterns of these two samples are identical and match well with JCPDS file no. 72−0274 in the tetragonal system with cell parameters a = 7.100 Å, c = 6.270 Å, and $\alpha = \beta = \gamma$, which confirms the pure phase formation of the prepared samples. The sharp and intense peaks of XRD patterns show the pure crystalline nature of the synthesized sample. The average crystallite size (D) of crystals grown is calculated using the Scherrer equation[19]

$$D = k\lambda/\beta \cos\theta$$

where k = 0.89, λ is the wavelength of Cu Kα radiation, β is the corrected full width at half-maximum of the diffraction peak in radians, and θ is the diffraction angle. The values of average crystallite sizes of phosphors synthesized by combustion and sol−gel are 39.2 and 53.8 nm, respectively. The average crystallite size is larger in the phosphor synthesized by sol−gel than that by the combustion method.

A comparative study of the crystalline behavior of phosphors synthesized by three different methods (i.e., combustion, sol−gel, and solid-state reaction methods) has been performed and is shown in Figure 1b. On heating the phosphors synthesized by combustion and sol−gel methods also at 1473 K, the crystallinity increases. The crystallinity is more for the phosphor synthesized by the solid-state reaction method than by the other two methods. The crystallite sizes of YVO_4:Ho^{3+},Yb^{3+} phosphors synthesized by combustion, sol−gel, and solid-state reaction methods are 57.62, 65.43, and 55.42 nm, respectively.

Figure 2 shows the SEM images of the YVO_4:Ho^{3+},Yb^{3+} phosphors synthesized by combustion and sol−gel methods. The histograms for the particle size distributions are shown in Figure 3, and the average particle size has been calculated using these histograms. The surface particles are random in shape, as shown in Figure 2a. However, the particles are well separated to each other and the average particle size is nearly equal to 0.54 μm for the YVO_4:Ho^{3+},Yb^{3+} phosphor synthesized by the combustion method at 973 K (see Figure 3a). When the phosphor sample is heated at 1473 K, the surface particles are modified toward a nearly spherical shape and the average size is increased to around 1.90 μm (see Figure 2c).

Figure 2b shows the SEM image of the YVO_4:Ho^{3+},Yb^{3+} phosphor synthesized via the sol−gel method at 973 K, in which the surface particles are again random in shape and agglomerated together. The average particle size is around 0.59 μm. The particles on the surface are modified toward a purely spherical shape on heating at 1473 K, and the average size is nearly 1.94 μm. This modification in shape and increase in particles size with an increase in temperature may be responsible for the enhancement of the overall emission as discussed in upcoming sections.

A comparative study of SEM images of all of the three samples synthesized by three different methods is shown in Figure 4. From the figure, it can be seen that the surface morphology of the particles of the phosphor sample synthesized by the sol−gel method is more spherical in shape than that of the samples synthesized by the other two methods at 1473 K.

A comparative study of the particle size distribution is shown as histograms from the SEM images of all three samples synthesized by three different techniques in Figure 5. The average particle sizes are 1.90, 1.94, and 1.53 μm in the cases of combustion, sol−gel, and solid-state reaction methods, respectively, when the samples are heated at 1473 K. However, the average particle sizes of samples prepared by sol−gel or by combustion methods at 973 K are much smaller.

2.2. Optical Properties. *2.2.1. Fourier Transform Infrared (FTIR) Measurement.* Figure 6 shows FTIR spectra of the samples synthesized in different ways and heated to different temperatures to study the vibrational behavior of the phosphor samples. The vibrational behavior of the YVO_4:Ho^{3+},Yb^{3+} phosphor synthesized the by solution combustion method is shown in Figure 6a. The vibrational peaks are observed at 453 and 776 cm^{-1} due to Y−O and V−O vibrations.[20] Some

DOI: 10.1021/acsomega.8b03606
ACS Omega 2019, 4, 6903−6913

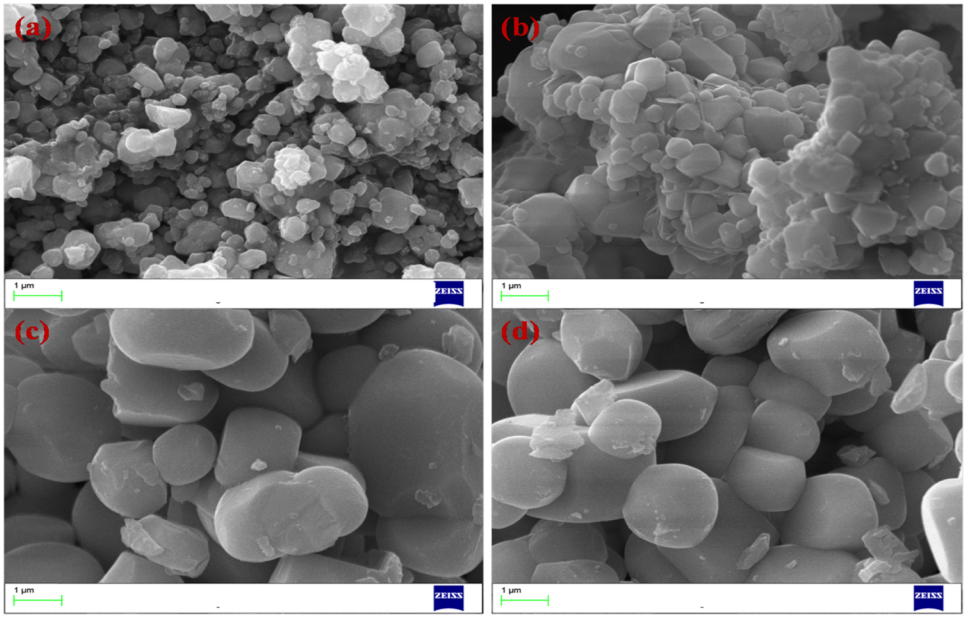

Figure 2. SEM images of YVO_4:Ho^{3+},Yb^{3+} synthesized by the (a) combustion method at 973 K, (b) sol−gel method at 973 K, (c) combustion method at 1473 K, and (d) sol−gel method at 1473 K.

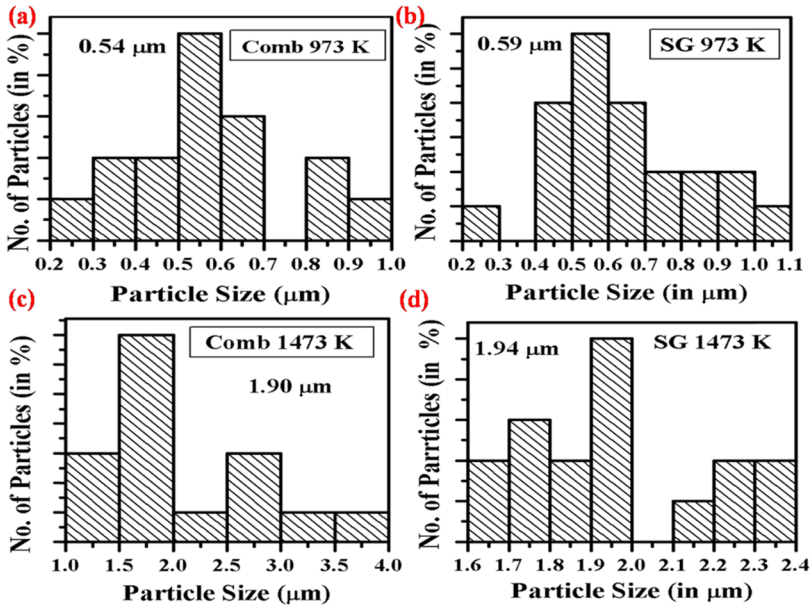

Figure 3. Histograms for the particle size distribution of YVO_4:Ho^{3+},Yb^{3+} synthesized by the (a) combustion method at 973 K, (b) sol−gel method at 973 K, (c) combustion method at 1473 K, and (d) sol−gel method at 1473 K.

additional peaks such as at 1011 and 1062 cm^{-1} due to C−O and at 1370 cm^{-1} due to nitrate groups are observed. When the YVO_4:Ho^{3+},Yb^{3+} phosphor is heated at 1473 K, the peaks due to C−O and nitrate groups disappeared. The peak due to V−O splits into two peaks, positioned at 760 and 830 cm^{-1}, which may be due to increased crystallinity at higher temperatures. Reduction in quenching centers as well as the absorbance intensity due to the V−O group may be responsible for the enhancement in the overall optical emission intensity. Figure 6b shows the FTIR spectra of the YVO_4:Ho^{3+},Yb^{3+} phosphor synthesized by the sol−gel technique. In this, all of the vibrational peaks show the same characteristics as discussed earlier except that the peak due to V−O vibration shifts toward the lower wave number side at 770 cm^{-1}.

A comparative study of vibrational behavior of YVO_4:Ho^{3+},Yb^{3+} phosphors synthesized by combustion, sol−gel, and solid-state reaction methods and heated to 1473 K is shown in Figure 6c. The characteristic spectra are nearly the same. The difference in all three spectra is that the peak due to V−O vibration is lower for the phosphor sample synthesized by the sol−gel method and the absorption intensity of the band due to the V−O group is weaker than that in the other two cases.

2.2.2. UV−Vis Absorption Measurement. Figure 7 shows the UV−vis−NIR absorption spectra of YVO_4:Ho^{3+},Yb^{3+} phosphors synthesized by three different methods in diffuse

DOI: 10.1021/acsomega.8b03606
ACS Omega 2019, 4, 6903−6913

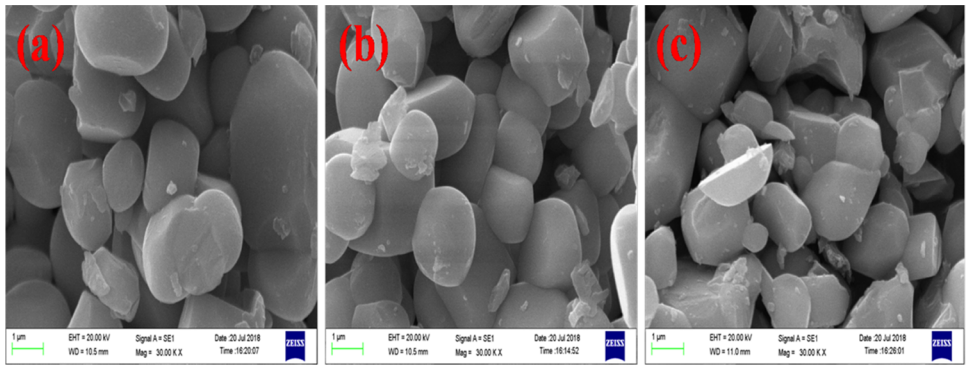

Figure 4. SEM images of YVO_4:Ho^{3+},Yb^{3+} phosphors synthesized by (a) combustion, (b) sol−gel, and (c) solid-state reaction methods at 1473 K.

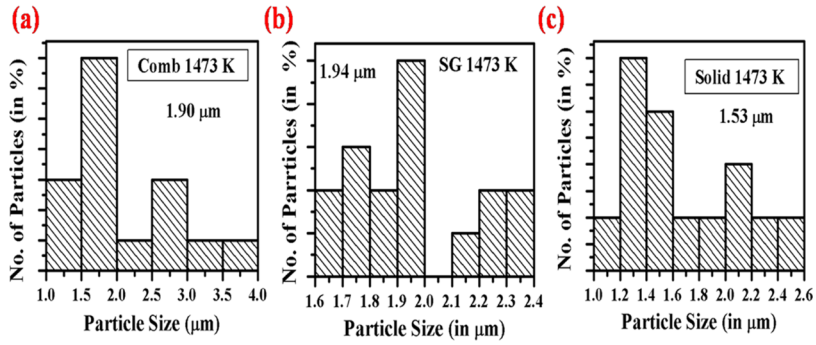

Figure 5. Histograms for the particle size distribution of YVO_4:Ho^{3+},Yb^{3+} phosphors synthesized by (a) combustion, (b) sol−gel, and (c) solid-state reaction methods at 1473 K.

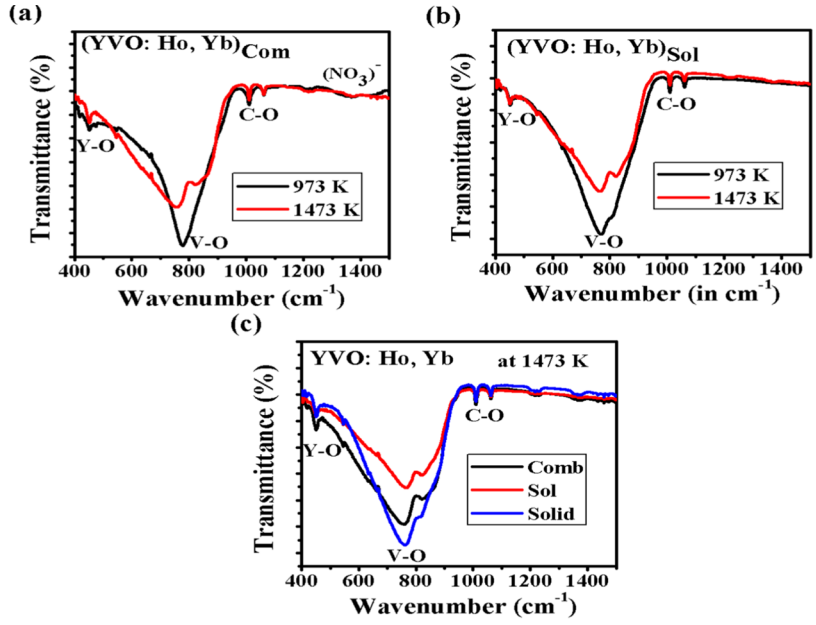

Figure 6. FTIR spectra of the YVO:Ho,Yb phosphor synthesized by the (a) combustion method at 973 and 1473 K, (b) sol−gel method at 973 and 1473 K, and (c) all three methods (i.e., combustion, sol−gel, and solid-state methods) at 1473 K.

reflectance mode. The absorption spectrum of the YVO:Ho,Yb phosphor synthesized by the combustion method at 973 K is shown in Figure 7a. There is a strong absorption band at 323 nm due to CTB of the $(VO_4)^{3-}$ group, and no sharp peaks are seen due to the f−f transition of the Ho^{3+} ion. When the phosphor sample is heated at 1473 K, the sharp peaks are observed at 456, 540, and 650 nm due to $^5I_8 \rightarrow {}^5G_6$, $^5I_8 \rightarrow {}^5F_4/{}^5S_2$, and $^5I_8 \rightarrow {}^5F_5$ transitions of the Ho^{3+} ion. This suggests that on heating the transition probability increases, which causes the enhancement in overall emission with temperature. Figure 7b shows the absorption spectrum of the YVO:Ho,Yb phosphor synthesized by the sol−gel technique. In this, the characteristics of the absorption spectra show a similar type of nature as discussed above.

Figure 7c shows a comparative study of UV−vis−NIR absorption spectra of the three YVO:Ho,Yb phosphor samples

DOI: 10.1021/acsomega.8b03606
ACS Omega 2019, 4, 6903−6913

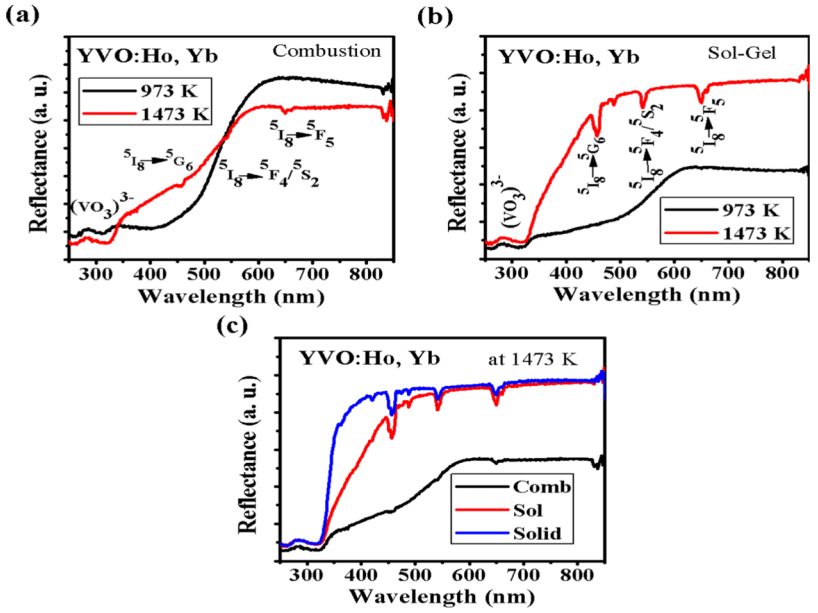

Figure 7. UV−vis absorption spectra of the YVO_4:Ho^{3+},Yb^{3+} phosphor synthesized by the (a) combustion method, (b) sol−gel method, and (c) all three methods at 1473 K.

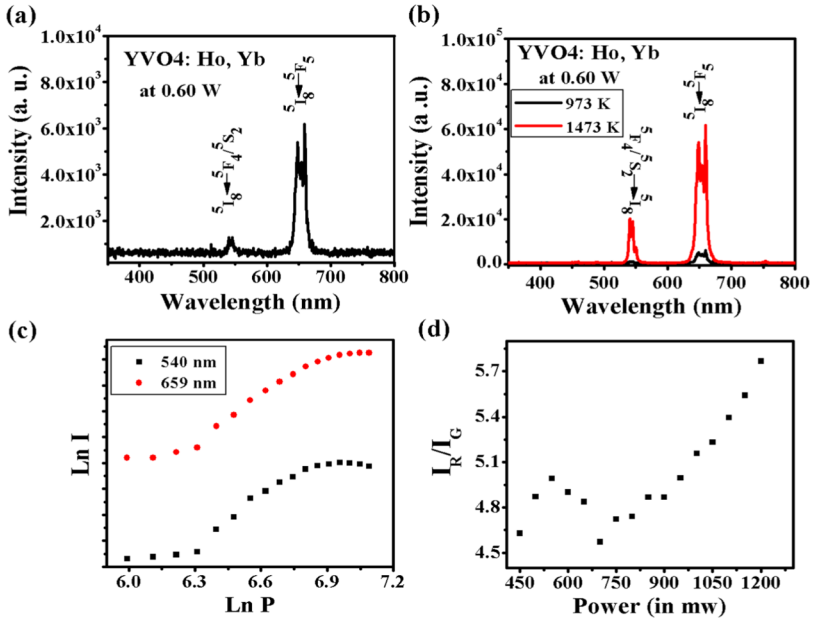

Figure 8. (a) UC emission spectrum of YVO_4:Ho^{3+},Yb^{3+} on excitation with a 980 nm laser at 0.6 W; (b) UC emission spectrum of YVO_4:Ho^{3+},Yb^{3+} on excitation with a 980 nm laser at 0.6 W pump power and heating at 973 and 1473 K; (c) power dependence study of green and red emissions; and (d) plot between the I_R/I_G ratio and pump power.

synthesized by three different techniques at 1473 K. In all of the three spectra, the absorption peaks of the YVO:Ho,Yb phosphor synthesized by the sol−gel technique show strong absorption as compared to those for other two methods. Thus, the intensity of the overall emission is more prominent in YVO:Ho,Yb synthesized by the sol−gel method.

2.2.3. Photoluminescence Behavior. 2.2.3.1. Upconversion Emission. 2.2.3.1.1 Combustion Method Figure 8a shows the UC emission spectra of the YVO_4:Ho^{3+},Yb^{3+} phosphor sample prepared at 973 K on excitation with a 980 nm diode laser at 0.60 W pump power synthesized by the solution combustion method. There is a weak green emission at 540 nm due to $^5F_4/^5S_2 \rightarrow {}^5I_8$ and intense red emission at 659 nm due to the $^5F_5 \rightarrow {}^5I_8$ transition of the Ho^{3+} ion. When the phosphor sample is heated to 1473 K, the overall UC emission intensity enhances significantly (see Figure 8b). The enhancement in green emission is nearly eight times and in red emission is nearly nine times. Along with this, there are weak emissions at 456 and 756 nm also due to $^4G_6 \rightarrow {}^5I_8$ and $^5F_4/^5S_2 \rightarrow {}^5I_7$ transitions of the Ho^{3+} ion in the heated YVO_4:Ho,Yb phosphor sample. This increase in the UC emission intensity on heating the sample may be due to the following reasons. The first reason is the quenching centers like carbonates, nitrates, etc. that are removed after heating the phosphor sample.[21] The second reason may be the modification in the

DOI: 10.1021/acsomega.8b03606
ACS Omega 2019, 4, 6903−6913

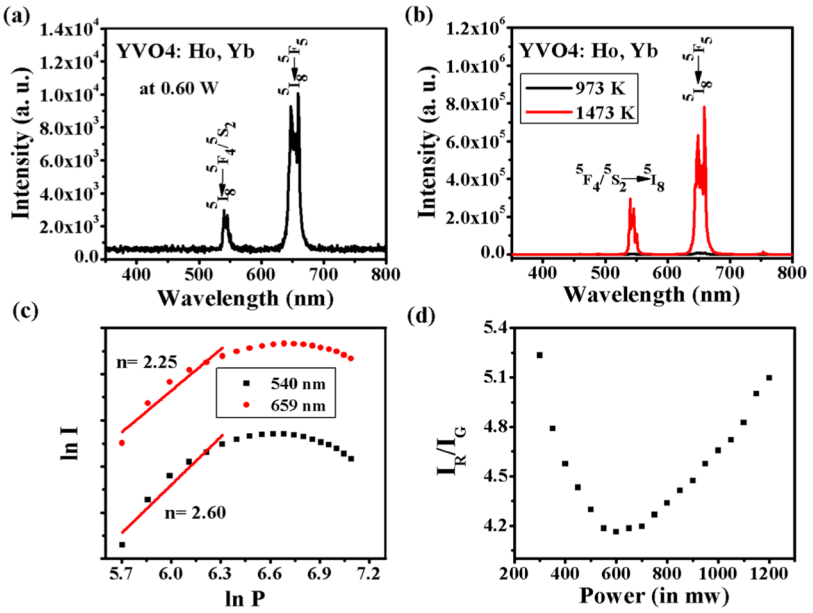

Figure 9. (a) UC emission spectrum of the YVO_4:Ho^{3+},Yb^{3+} phosphor sample prepared by the sol−gel method on excitation with a 980 nm laser at 0.6 W pump power; (b) UC emission spectrum of YVO_4:Ho^{3+},Yb^{3+} on excitation with a 980 nm laser at 0.6 W and heating at 973 and 1473 K; (c) power dependence study of green and red emissions; and (d) plot between the I_R/I_G ratio and pump power.

shape and size of the particles in the synthesized phosphor at 1473 K.[22]

Figure 8c shows the power-dependent study of YVO_4:Ho,Yb for two different transitions at 540 and 659 nm. Since the UC process is a nonlinear phenomenon related to I_{uc} α $(P_{in})^n$, where n is the number of photons involved in a particular transition.[23] In Figure 8c, the log−log plot of the UC emission intensity and the pump power gives the value of slope (n). Initially, the emission intensity varies linearly with pump power. It rises suddenly, and the value of slope (n) increases significantly after certain threshold pump power. This behavior is known as the photon avalanche UC process.[24] At higher pump power, saturation occurs and a decrease in slope suggests that there is prominent heating in the material. Figure 8d shows the variation of the I_R/I_G ratio with the pump power of diode laser. There are three regions in this: In the first region, the ratio increases up to certain pump power (i.e., 500 mW), which is due to low photon density. Thus, the lower levels are populated more than the higher levels and the red emission intensity increases. In the second region, the ratio decreases up to certain power (≈700 mW) of diode laser due to high photon density, which enhances the population of higher levels, thereby increasing the green emission intensity. The third region shows a rapid increase in the ratio with pump power. It has been reported in the literature that heating becomes more prominent at higher pump power and multiphonon relaxation increases.[25,26] Due to this, the relaxation from the green-emitting level to a lower-lying red-emitting level increases. Thus, the intensity of red emission increases. This causes an increase in the ratio with pump power.

2.2.3.1.2 Sol−Gel Method Figure 9a shows the UC emission spectrum of the YVO_4:Ho^{3+},Yb^{3+} phosphor sample synthesized by the sol−gel method and heated at 973 K on excitation with a 980 nm diode laser at 0.6 W pump power. The emission peaks are at 540, 546, and 659 nm due to $^5F_4 \rightarrow {}^5I_8$, $^5S_2 \rightarrow {}^5I_8$, and $^5F_5 \rightarrow {}^5I_8$ transitions of the Ho^{3+} ion, respectively. The green emission at 540 nm in this case is more prominent than in the phosphor sample prepared by the combustion method. The overall emission intensity increases several times on heating the sample at 1473 K, as shown in Figure 9b. The enhancements in Green and Red emissions are nearly 63 and 56 times, respectively. The reason for the enhancement may be the same as discussed in the earlier case. It has been already observed in the SEM image that the particle size increases and shape is also modified toward nearly spherical. Due to increase in size, the separation between the activator and the sensitizer decreases, which increases the possibility of the energy transfer between them. Thus, the emission intensity is enhanced several times.

Figure 9c shows the log−log plot between the UC emission intensity at two different wavelengths and the power of the incident radiation. The slope gives the number of photons involved in green and red emissions. The values of "n" are 2.60 for green and 2.25 for red emissions. This suggests the contribution of the process involving more than two photons for green emission and 2 photons for red emission. This study is also helpful in explaining the mechanism for UC emission by using an energy-level diagram, which will be discussed in the next section. From the energy-level diagram, it seems that the involvement of photons in green emission should be 2. However, in the present case, it is more than 2, which may be due to the fast multiphonon relaxation from the $^5I_6$ level to the $^5I_7$ level and also from $^5F_4$ and $^5S_2$ levels to the $^5F_5$ level. At higher pump powers, there is heating in the material, which is termed as laser-induced optical heating. Therefore, multi-phonon relaxation becomes dominant and emission intensity decreases, which result in a negative slope.

The variation of the I_R/I_G ratio with respect to the pump power of the incident radiation (i.e., 980 nm diode laser) is shown in Figure 9d. This variation gives very important views about the UC emission mechanism with pump power. From the figure, it can be seen that there are two regions. In the first region, the I_R/I_G ratio decreases with an increase in the pump power up to a certain limit (≈600 mW). Actually, with the increase of pump power, the photon density increases, which

DOI: 10.1021/acsomega.8b03606
ACS Omega 2019, 4, 6903−6913

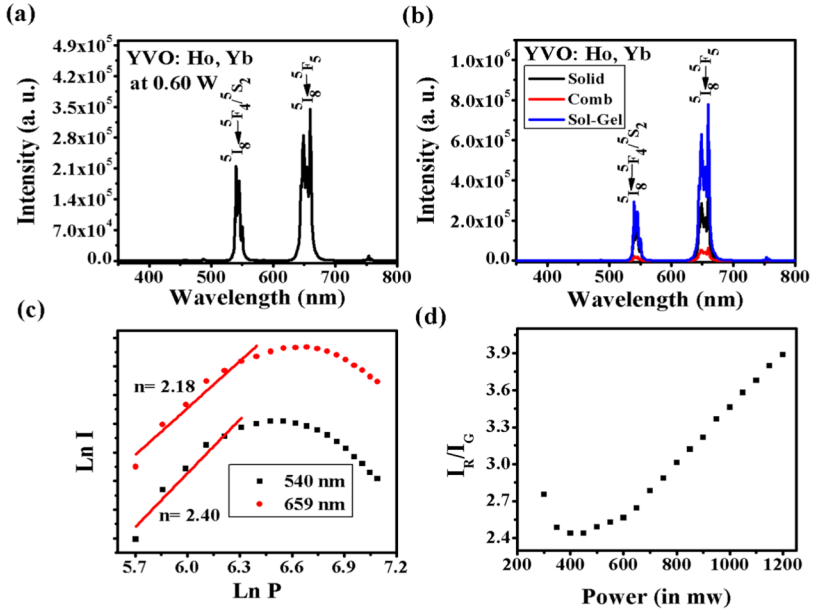

Figure 10. (a) UC emission spectra of the YVO_4:Ho^{3+},Yb^{3+} phosphor material prepared by the solid-state reaction method on excitation with a 980 nm laser at 0.6 W pump power; (b) comparison of UC emission spectra of the YVO_4:Ho^{3+},Yb^{3+} phosphor prepared by different techniques at 1473 K; (c) power dependence study of UC emission in the case of sample prepared by the solid-state reaction method; (d) variation of the I_R/I_G ratio with power in the case of sample prepared by the solid-state reaction method.

increases the population in the $^5F_4$ and $^5S_2$ levels, and green emission intensity increases. After certain pump power (>600 mW), the heating in the material increases due to laser-induced optical heating. Due to this, the multiphonon relaxation increases. Thus, the Ho^{3+} ions in $^5F_4/^5S_2$ levels relax rapidly to the $^5F_5$ level. Due to this, the lower level $^5F_5$ is increasingly populated. This causes an increase in the emission intensity of the red line at higher pump power. Thus, pump power can be used to tune the emission from green to red.

2.2.3.1.3 Solid-State Reaction Technique The upconversion emission spectrum of the YVO_4:Ho^{3+},Yb^{3+} phosphor sample prepared by the solid-state reaction method at 1473 K on excitation with a 980 nm diode laser at 0.6 W pump power is shown in Figure 10a. The characteristic spectrum is similar to that explained previously. In this case, the green emission intensity is more prominent as compared to that in the other two phosphor samples synthesized by other two techniques. This increase in the green emission compared to others is due to increase in size of particles and negligible quenching centers at 1473 K. Figure 10b shows a comparative study of the UC emission spectra of all of the three samples prepared by three different techniques and calcined at 1473 K. This shows that the phosphor synthesized by the sol−gel technique gives overall more intense emission as compared with the other two techniques. Actually, in the samples synthesized by sol−gel and combustion techniques at 973 K, the particles are in nano range size. After heat treatment to the prepared phosphor samples at 1473 K, the particle size increases and the shape is also modified. In the sample synthesized via the sol−gel method, the size of the particle increases and the shape is also modified toward nearly spherical. A comparison between all three phosphor samples synthesized via three different techniques shows that the size of the particles is larger and the particles are more spherical in the case of the sol−gel technique than in the other two techniques. The modification in shape and size of the surface particles supports the variation in the UC emission intensity. The samples with nearly spherical shape show more prominent UC emission intensity due to less scattering of the incident radiation.[22] Another reason of the increment in UC emission intensity is the increment in particle size at 1473 K. Silver et al.[15] have reported that the sample with larger particle size shows more emission intensity.

Figure 10c shows the power-dependent emission intensity to calculate the number of photons involved in the green (540 nm) and red (659 nm) UC emissions. Its value is 2.40 for green and 2.18 for red emission. This suggests the involvement of two photons for both emissions. The value of *n* decreases at a higher pump power, which suggests laser-induced optical heating in the sample. The variation of the I_R/I_G ratio with pump power is shown in Figure 10d. First, the ratio decreases up to 400 mW pump power and then increases with pump power. This means that at lower pump power green emission intensity increases with the pump power up to 400 mW, then, it saturates, and finally decreases at higher power. At higher pump power, the ions are excited to $^5F_4/^5S_2$ and then relax to populate the $^5F_5$ level to give red emission. The reason behind this behavior is explained earlier.

From power dependence study of all of the three phosphor samples synthesized by different techniques, it is observed that the phosphor synthesized by the combustion technique shows a tendency toward the photon avalanche process after certain threshold pump power and laser-induced optical heating is observed at high power. However, in the case of the other two phosphors synthesized by sol−gel and solid-state methods, there is no photon avalanche process; however, heating is observed at comparatively low pump power. Another interesting observation is that relaxation at higher power is more prominent in the case of the green-emitting level than for the red-emitting level.

2.2.3.1.4 Mechanism Involved in Upconversion Emission Figure 11 shows the energy-level diagram to explain the mechanism involved in the UC emission on excitation with a 980 nm diode laser. In the present system, the Yb^{3+} ion acts as a

DOI: 10.1021/acsomega.8b03606
ACS Omega 2019, 4, 6903−6913

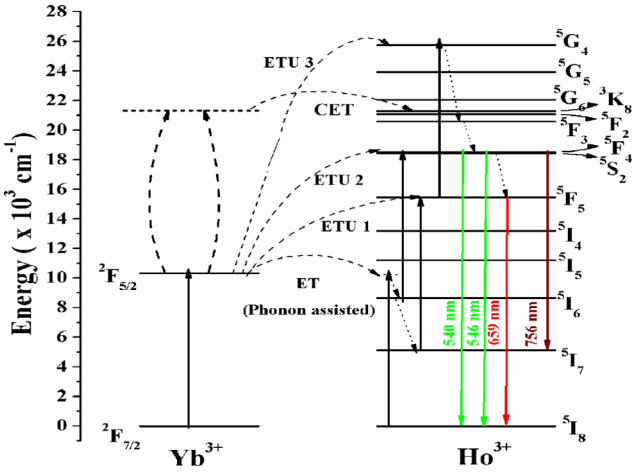

Figure 11. Possible energy-level diagram to explain the upconversion emission behavior of the YVO_4:Ho^{3+},Yb^{3+} phosphor.

sensitizer and the Ho^{3+} ion is an activator. When the Ho^{3+}/Yb^{3+}-codoped YVO_4 phosphor is irradiated by a 980 nm diode laser, the Yb^{3+} ion absorbs the incident radiation strongly due to its higher absorption cross section for 980 nm wavelength than that of the Ho^{3+} ion. The deexcitation energy of the Yb^{3+} ion is transferred to the Ho^{3+} ion. However, due to mismatch in the energy levels of the two ions, the energy transfer will be phonon-assisted one. The Ho^{3+} ion in the ground state ($^5I_8$) is promoted to $^5I_6$ via phonon-assisted energy transfer. The Ho^{3+} ion in the $^5I_6$ level absorbs second photon and promoted to the $^5F_4/^5S_2$ level via the ESA/ETU process. Thus, various transitions observed in green and red regions are represented as

$$^2F_{7/2}(Yb^{3+}) + h\nu \rightarrow {}^2F_{5/2}(Yb^{3+})$$

$$^2F_{5/2}(Yb^{3+}) + {}^5I_8(Ho^{3+}) \rightarrow {}^2F_{7/2}(Yb^{3+}) + {}^5I_6(Ho^{3+})$$

$$^2F_{5/2}(Yb^{3+}) + {}^5I_6(Ho^{3+}) \rightarrow {}^2F_{7/2}(Yb^{3+}) + {}^5F_4/{}^5S_2(Ho^{3+})$$

There may be several other channels also for the UC emission from various other excited levels. There are various quenching centers also present in the system. Thus, the strong nonradiative relaxation takes place from $^5I_6$ to $^5I_7$. The ions in the $^5I_7$ level absorb the second incident photon and promoted to the $^5F_5$ level via the ETU/ESA process. After absorbing the third photon, the Ho^{3+} ions are promoted to the $^5G_4$ level. The relaxation from this high-lying level to $^5F_4/^5S_2$ and $^5F_5$ levels gives emission in green and red regions. The mechanism can be represented as

$$^2F_{5/2}(Yb^{3+}) + {}^5I_8(Ho^{3+}) \rightarrow {}^2F_{7/2}(Yb^{3+}) + {}^5I_6(Ho^{3+})$$

$$^5I_6(Ho^{3+}) \rightarrow {}^5I_7(Ho^{3+}) \text{ (via relaxation process)}$$

$$^2F_{5/2}(Yb^{3+}) + {}^5I_7(Ho^{3+}) \rightarrow {}^2F_{7/2}(Yb^{3+}) + {}^5F_5(Ho^{3+})$$

$$^2F_{5/2}(Yb^{3+}) + {}^5F_5(Ho^{3+}) \rightarrow {}^2F_{7/2}(Yb^{3+}) + {}^5G_4(Ho^{3+})$$

The samples prepared by sol−gel and combustion methods follow this mechanism to build up population in higher levels. Therefore, the green emission is very weak as compared to the red emission in the YVO:Ho^{3+},Yb^{3+} phosphor synthesized by these two different techniques.

Another channel for the UC emission is cooperative energy transfer between two Yb^{3+} ions and one Ho^{3+} ion. In this process, two excited Yb^{3+} ions interact simultaneously with one Ho^{3+} in the ground state and transfer their energies to Ho^{3+} to promote it to the $^5F_2$ level. The relaxation from this level to lower levels gives various transitions in different regions.

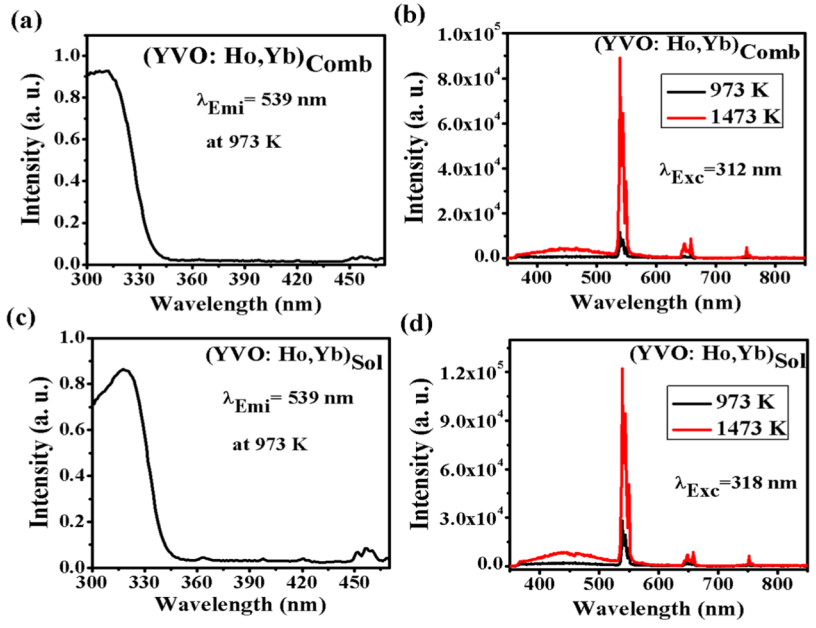

Figure 12. (a) PLE spectrum of the YVO_4:Ho^{3+},Yb^{3+} phosphor synthesized by the combustion method at 973 K by monitoring emission at 539 nm, (b) PL emission spectra of the YVO_4:Ho^{3+},Yb^{3+} phosphor synthesized by the combustion method at 973 and 1473 K on excitation with a 312 nm laser, (c) PLE spectrum of the YVO_4:Ho^{3+},Yb^{3+} phosphor synthesized by the sol−gel method at 973 K by monitoring emission at 539 nm, and (d) PL emission spectra of the YVO_4:Ho^{3+},Yb^{3+} phosphor synthesized by the sol−gel method at 973 and 1473 K on excitation with a 318 nm laser.

DOI: 10.1021/acsomega.8b03606
ACS Omega 2019, 4, 6903−6913

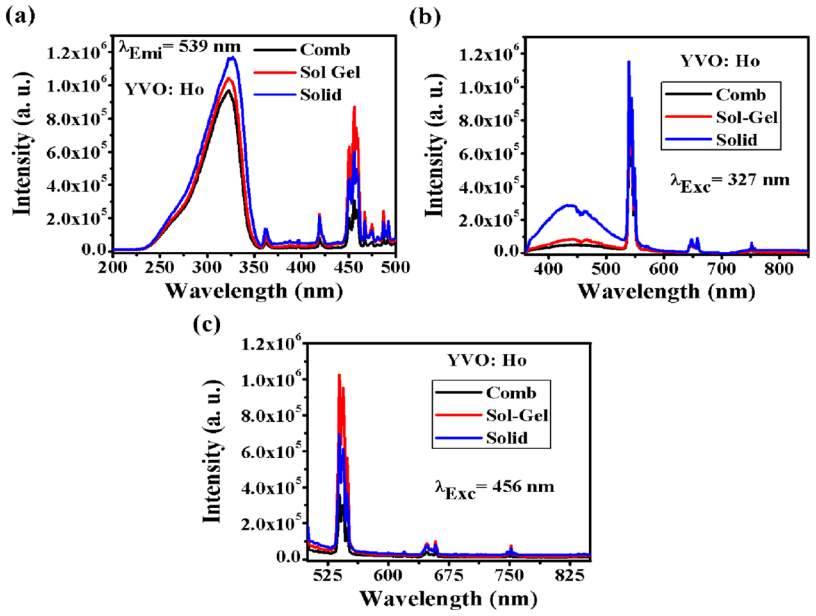

Figure 13. (a) PLE spectra of the YVO_4:Ho^{3+},Yb^{3+} phosphor synthesized by three different methods at 1473 K by monitoring emission at 539 nm; PL emission spectra of YVO_4:Ho^{3+},Yb^{3+} phosphor synthesized by three different methods at 1473 K on excitation with (b) 327 nm and (c) 456 nm laser.

$$2\ {}^2F_{5/2}(Yb^{3+}) + {}^5I_8(Ho^{3+}) \rightarrow 2\ {}^2F_{7/2}(Yb^{3+}) + {}^5F_2(Ho^{3+})$$

A nonradiative relaxation from these levels to $^5F_4/^5S_2$ gives green emission. However, this channel is not as effective as the other two channels.

2.2.3.2. Downshifting Emission. Figure 12 shows the downshifting behavior of Ho^{3+}-doped YVO_4 phosphor samples synthesized by two different methods (i.e., solution combustion and sol−gel methods). Figure 12a shows the photoluminescence excitation (PLE) spectra of the YVO_4:Ho^{3+},Yb^{3+} phosphor synthesized by the combustion method with λ_{Emi} = 539 nm. There is a broad peak at 312 nm due to the charge transfer band of the $(VO_4)^{3-}$ group and a weak sharp peak at 456 nm due to the $^5I_8 \rightarrow {}^5G_6$ transition of the Ho^{3+} ion. On excitation with a 312 nm laser, there is a broad photoluminescence peak at 450 nm due to the $(VO_4)^{3-}$ group, which suggests that this host is a self-activated host. In addition to a broad peak, there appears a large number of sharp peaks at 539, 663, and 756 nm due to $^5F_4/^5S_2 \rightarrow {}^5I_8$, $^5F_5 \rightarrow {}^5I_8$, and $^5F_4 \rightarrow {}^5I_7$ transitions of the Ho^{3+} ion. It is interesting to note that whereas in the UC process the sample gives intense red emission, in DS, it gives intense green and weak red emissions. This is due to the change in the channel of the excitation of Ho^{3+} ions.

When the phosphor sample is heated at 1473 K, the overall emission of the host as well as the Ho^{3+} ion enhances significantly (see Figure 12b). This enhancement may be due to reduction in quenching centers at high temperature and due to modification in the shape and size of the particles. This has been justified by the enhancement in transition probability as observed in UV−vis absorption spectra and also by FTIR spectra. The mechanism behind the DS behavior is well explained by the energy-level diagram. Figure 12c,d shows the photoluminescence excitation and emission spectra of the YVO_4:Ho^{3+},Yb^{3+} phosphor synthesized by the sol−gel method. In this case also, the phosphor sample shows the same characteristic spectrum and behavior as explained in the phosphor synthesized by the combustion method.

In Figure 13, a comparative study of DS behaviors of YVO_4:Ho^{3+},Yb^{3+} phosphor samples synthesized by three different methods such as combustion, sol−gel, and solid-state reaction methods are reported at 1473 K. Figure 13a shows the PLE spectra of YVO_4:Ho^{3+},Yb^{3+} by monitoring the emission at 539 nm due to the $^5F_4/^5S_2 \rightarrow {}^5I_8$ transition of the Ho^{3+} ion synthesized by three different techniques. The CTB due to the $(VO_4)^{3-}$ group is observed in the UV region in all of the three cases. The peak value of CTB shifts toward the higher wavelength side (i.e., 312, 318, and 327 nm) in the case of samples synthesized by combustion, sol−gel, and solid-state methods, respectively. This shift may be due to change in the environment after the synthesis of the sample. The CTB is more intense in the phosphor synthesized by the solid-state reaction method. It can also be observed in Figure 13b that the emission from the $(VO_4)^{3-}$ group is more prominent for the same sample. Therefore, overall emission is more intense for the same sample due to energy transfer from the $(VO_4)^{3-}$ group to the Ho^{3+} ion on excitation with a 327 nm diode laser. Figure 13c shows the comparative emission spectra of phosphor samples synthesized by three different methods on excitation with a 456 nm diode laser. In this case, the sample synthesized by the sol−gel method at 1473 K gives more intense DS behavior. This may be due to increase of particle size in the sample prepared by the sol−gel method, as explained earlier, and also the absence of quenching centers.[1]

The mechanism behind this DS behavior is well explained by a possible energy-level diagram, as shown in the Figure 14. The $(VO_4)^{3-}$ group is excited on excitation with a 327 nm laser. The emission from the $(VO_4)^{3-}$ group is observed in the broad blue region at 450 nm. There is resonant energy transfer from the $(VO_4)^{3-}$ group to the $^5G_4$ level of the Ho^{3+} ion. The Ho^{3+} ions relax from that level to lower-lying levels and give various emissions in different wavelengths. When the phosphor sample is excited with a 456 nm laser, the Ho^{3+} ion is promoted to the

DOI: 10.1021/acsomega.8b03606
ACS Omega 2019, 4, 6903−6913

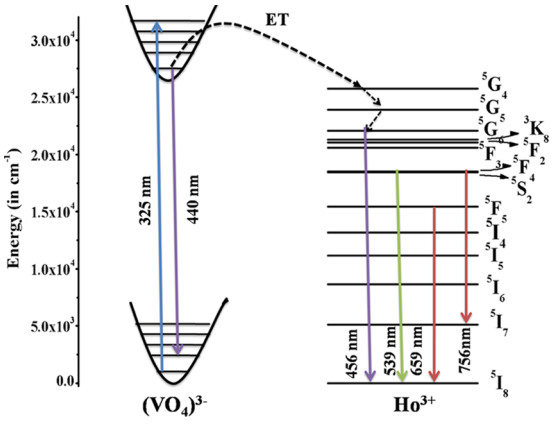

Figure 14. Possible energy-level diagram to explain the mechanism behind the DS behavior.

$^5G_6$ level directly. The relaxation from this level to low-lying levels gives various emissions in different regions.

3. CONCLUSIONS

Ho^{3+}/Yb^{3+}-codoped YVO_4 phosphors have been synthesized using three different techniques. SEM images show the modification in shape and size of the surface particles synthesized by different techniques and also by heating all of the samples at 1473 K. The intensity of the vibrational peaks reduces on annealing the samples at 1473 K synthesized by sol−gel/combustion methods. The UV−vis−NIR absorption spectra show only few and weak bands in the samples synthesized by sol−gel/combustion methods. However, these absorption bands are strong in the annealed samples. The UV−vis−NIR bands are maximum for the phosphor synthesized by the sol−gel method. The UC emission in Ho^{3+}/Yb^{3+}-codoped YVO_4 phosphors synthesized by combustion and sol−gel techniques at 973 K shows intense red and weak green emissions. The UC emission intensity increases significantly about 65 times in green and 56 times in red emission on heating the phosphor at 1473 K in the phosphor sample synthesized by the sol−gel method. This enhancement in the overall UC emission is also due to increase in particle size and also modification in the shape of particles toward nearly spherical. The intense red emission in such a material can be used for the bioimaging application. The same samples in the DS process emit intense green and weak red bands. The enhancement is also observed in DS behavior of the material at higher temperature. Thus, the phosphor sample synthesized by the sol−gel technique gives better optical properties.

4. EXPERIMENTAL METHODS

4.1. Chemicals Used. Analytical-grade yttrium oxide (Y_2O_3, 99.9%, Alfa-Aesar), vanadium pentoxide (V_2O_5, 99.9%, Himedia), holmium oxide (Ho_2O_3, 99.99%, Alfa-Aesar), and ytterbium oxide (Yb_2O_3, 99.99%, Alfa-Aesar) were used for the synthesis of $Y_{0.94}Ho_{0.01}Yb_{0.05}VO_4$ (YVO:-Ho,Yb) phosphor samples using three different techniques.

4.2. Synthesis of Phosphors. The phosphor samples were synthesized using three different techniques:

4.2.1. Solution Combustion Method. All of the oxide samples in their stoichiometric proportions were dissolved in nitric acid to form their nitrates. The nitrates thus formed were mixed with each other properly and then with urea. The mixture was then kept on a magnetic stirrer at 353 K and stirred till it was converted into a gel. The gel was then transferred to a crucible and placed in an electric furnace where the combustion was carried out at 973 K. During combustion, different gases were released and the gel was converted into a foamlike material. The material was then grinded in an agate mortar, which gave us the final compound for further measurements. A part of this sample was heated to 1473 K for 4 h. Thus, there are two samples prepared by this method on (I) heating at 973 K and (II) heating at 1473 K.

4.2.2. Sol−Gel Method. In this method,[17] all of the chemicals in the oxide form in stoichiometric proportion were converted into the nitrate form as in the earlier case. The nitrate forms of these chemicals were mixed together properly. The citric acid in 2:1 ratio and polyethylene glycol (molecular weight 8000) were added to this mixture. The resultant mixture was stirred for 1 h for homogeneous mixing, and then, the whole mixture was heated at 348 K in a water bath for the formation of a homogeneous gel. The gel was kept in the oven at 383 K for 12 h to form a powder sample. Then, the powder sample was fired at 973 and 1473 K for 4 h.

4.2.3. Solid-State Reaction Method. In this technique,[18] the stoichiometric amounts of pure starting oxide materials were thoroughly mixed in an agate mortar for nearly 1 h to form a homogeneous mixture using nearly 50 ml of acetone as a mixing medium. The homogeneous mixture was placed in an alumina crucible, heated in an electric furnace at 1473 K temperature for 4 h, and then cooled to room temperature. The phosphor sample thus obtained was crushed to get fine powder of the phosphor for further studies.

Thus, there are five samples for further studies.

4.3. Characterizations. The X-ray diffraction patterns of all of the five powder phosphor samples were monitored using an 18 kW Cu rotating anode-based high-resolution Rigaku X-powder (XRD) diffractometer. The surface morphology of the samples was monitored using a scanning electron microscope (SEM) unit [ZEISS (SEM-Supra40 model)] operated at 20 kV. The vibrational structure of the synthesized phosphor samples was studied using a PerkinElmer FTIR spectrometer (Frontier) in the range 400−1500 cm^{-1}. UV−vis−NIR absorption measurements were carried out using a PerkinElmer UV/vis/NIR spectrometer [model Lambda 750] in the range 300−1100 nm. For DS measurements, a Fluorolog-3 model FL 3-11 (Horiba Jobin Yvon) spectrophotometer equipped with a 450 W xenon flash lamp was used. The UC luminescence spectra were obtained using a 980 nm tunable CW diode laser (2W, Model-III980, Chengchun New Industries optoelectronics tech. Co. Ltd.,) as an excitation source, and the emission was monitored using an iHR 320 (Horiba Jobin Yvon) spectrometer equipped with an R928P photomultiplier tube (PMT). All of the measurements of the samples have been carried out in the powder form at room temperature.

AUTHOR INFORMATION

Corresponding Authors

*E-mail: devendra.cer@itbhu.ac.in (D.K.).
*E-mail: sbrai49@yahoo.co.in (S.B.R.).

ORCID

Shyam B. Rai: 0000-0002-6321-1038

Notes

The authors declare no competing financial interest.

DOI: 10.1021/acsomega.8b03606
ACS Omega 2019, 4, 6903−6913

■ ACKNOWLEDGMENTS

One of authors, Dr. Abhishek Dwivedi, acknowledges the Indian Institute of Technology, BHU, for the financial assistance in terms of Institute Postdoctoral fellowship.

■ REFERENCES

(1) Jha, A.; Richards, B.; Jose, G.; Fernandez, T. T.; Joshi, P.; Jian, X.; Lousteau, J. Rare earth ion doped TeO2 and GeO2 glasses as laser materials. *Prog. Mater. Sci.* **2012**, *57*, 1426−1491.

(2) Pust, P.; Weiler, V.; Hech, C.; Tucks, A.; Wochnik, A. S.; Hen*β*, A. K.; Wiechert, D.; Scheu, C.; Schnidt, J.; Schnick, W. Narrow-band red emitting $Sr[LiAl_3N_4]:Eu^{2+}$ as a next generation LED phosphor materials. *Nat. Mater.* **2014**, *13*, No. 891.

(3) Ballato, J.; Lewis, J. S.; Holloway, P. Display applications of rare-earth-doped materials. *MRS Bull.* **1999**, *24*, 51−56.

(4) Han, B.; Liang, H.; Ni, H.; Su, Q.; Yang, G.; Shi, J.; Zhang, G. Intense red light emission of Eu^{3+}-doped $LiGd(PO_3)_4$ for mercury-free lamps and plasma display panels application. *Opt. Express* **2009**, *17*, 7138−7144.

(5) Wang, H. Q.; Batentschuk, M.; Osvet, A.; Pima, L.; Brabec, C. Rare-Earth Ion Doped Up-Conversion Materials for Photovoltaic Applications. *Adv. Mater.* **2011**, *23*, 2675−2680.

(6) Kumar, R.; Nyk, M.; Ohulchmsky, T. Y.; Flask, C. A.; Prasad, P. N. Combined optical and MR Bioimaging Using Rare Earth Ion Doped $NaYF_4$ Nanocrystals. *Adv. Funct. Mater.* **2009**, *19*, 853−859.

(7) Rai, V. K. Temperature sensors and optical sensors. *Appl. Phys. B* **2007**, *88*, 297−303.

(8) Niu, X.; Zhong, H.; Wang, X.; Jiang, K. Sensing properties of rare earth oxide doped In_2O_3 by a Sol-Gel method. *Sens. Actuators, B* **2006**, *115*, 434−438.

(9) Singh, A. K.; Singh, S. K.; Gupta, B. K.; Prakash, R.; Rai, S. B. Probing a highly efficient dual mode: down−upconversion luminescence and temperature sensing performance of rare-earth oxide phosphors. *Dalton Trans.* **2013**, *42*, 1065−1072.

(10) Dwivedi, A.; Singh, A. K.; Rai, S. B. Down-shifting and upconversion photoluminescence in Ho^{3+}/Yb^{3+} codoped $GdNbO_4$: effect of the Bi^{3+} ion and the magnetic field. *Dalton Trans.* **2014**, *43*, 15906−15914.

(11) Yi, G.; Lu, H.; Zhao, S.; Ge, Y.; Yang, W.; Chen, D.; Guo, L. H. Synthesis, Characterization, and Biological Application of Size-Controlled Nanocrystalline NaYF4:Yb,Er Infrared-to-Visible Up-Conversion Phosphors. *Nano Lett.* **2004**, *4*, 2191−2196.

(12) Shea, L. E.; Mckittrick, J.; Lopez, O. A. Synthesis of Red-Emitting, Small Particle Size Luminescent Oxides Using an Optimized Combustion Process. *J. Am. Ceram. Soc.* **1996**, *79*, 3257−3265.

(13) Lee, S.; Song, D.; Kim, D.; Lee, J.; Kim, S.; Park, I. Y.; Choi, Y. D. Effects of synthesis temperature on particle size/shape and photoluminescence characteristics of ZnS:Cu nanocrystals. *Mater. Lett.* **2004**, *58*, 342−346.

(14) Yu, M.; Lin, J.; Wang, Z.; Fu, J.; Wang, S.; Zhang, H. J.; Han, Y. C. Fabrication, Patterning, and Optical Properties of Nanocrystalline YVO4:A (A = $Eu^{3+}Dy^{3+}Sm^{3+}Er^{3+}$) Phosphor Films via Sol−Gel Soft Lithography. *Chem. Mater.* **2002**, *14*, 2224−2231.

(15) Silver, J.; Martinez-Rubio, M. I.; Ireland, T. G.; Fern, G. R.; Withnall, R. The Effect of Particle Morphology and Crystallite Size on the Upconversion Luminescence Properties of Erbium and Ytterbium Co-doped Yttrium Oxide Phosphors. *J. Phys. Chem. B* **2001**, *105*, 948−953.

(16) Wang, W. N.; Widiyastuti, W.; Ogi, T.; Lenggoro, I. W.; Okuyama, K. Correlations between Crystallite/Particle Size and Photoluminescence Properties of Submicrometer Phosphors. *Chem. Mater* **2007**, *19*, 1723−1730.

(17) Li, L.; Kyoung, H.; Moon, B. K.; Fu, Z.; Guo, C.; Jeong, J. H.; Li, S. S.; Jang, K.; Li, H. S. Photoluminescence Properties of $CeO_2:Eu^{3+}$ Nanoparticles Synthesized by a Sol-Gel Method. *J. Phys. Chem. C* **2009**, *113*, 610−617.

(18) Dwivedi, A.; Mishra, K.; Rai, S. B. Multi-modal luminescence properties of RE^{3+} (Tm^{3+}, Yb^{3+}) and Bi^{3+} activated $GdNbO_4$ phosphors—upconversion, downshifting and quantum cutting for spectral conversion. *J. Phys. D: Appl. Phys.* **2015**, *48*, No. 435103.

(19) Fu, Z.; Moon, B. K.; Yang, H. K.; Jeong, J. H. Synthesis, Characterization, and Luminescent Properties of Pr^{3+}-Doped Bulk and Nanocrystalline $BaTiO_3$ Phosphors. *J. Phys. Chem. C* **2008**, *112*, 5724−5728.

(20) Choi, S.; Moon, Y. M.; Jung, H. K. Luminescent properties of PEG-added nanocrystalline YVO4:Eu3+ phosphor prepared by a hydrothermal method. *J. Lumin.* **2010**, *130*, 549−553.

(21) Joshi, C.; Dwivedi, A.; Rai, S. B. Structural morphology, upconversion luminescence and optical thermometric sensing behavior of Y2O3:Er3+/Yb3+ nano-crystalline phosphor. *Spectrochim. Acta, Part A* **2014**, *129*, 451−456.

(22) Dwivedi, A.; Mishra, K.; Rai, S. B. Role of Gd^{3+} ion on downshifting and upconversion emission properties of Pr^{3+}, Yb^{3+} co-doped $YNbO_4$ phosphor and sensitization effect of Bi^{3+} ion. *J. Appl. Phys.* **2016**, *120*, No. 043102.

(23) Pollnau, M.; Gamelin, D. R.; Luthi, B. R.; Gudel, H. U. Power dependence of upconversion luminescence in lanthanide and transition-metal-ion systems. *Phys. Rev. B* **2006**, *61*, 3337−3346.

(24) Wang, X.; Xiao, S.; Bu, Y.; Yang, X.; Ding, J. W. Visible photon-avalanche upconversion in Ho^{3+} singly doped *β*-$Na(Y_{1.5}Na_{0.5})F_6$ under 980 nm excitation. *Opt. Lett.* **2008**, *33*, 2653−2655.

(25) Singh, A. K.; Kumar, K.; Pandey, A. C.; Rai, S. B.; Kumar, D. Multi-phonon assisted upconversion emission and power dependence studies in LaF3:Er3+ phosphor. *Spectrochim. Acta, Part A* **2013**, *106*, 236−241.

(26) Dwivedi, A.; Mishra, K.; Rai, S. B. Tm^{3+}, Yb^{3+} activated $ANbO_4$ (A = Y, Gd, La) phosphors: a comparative study of optical properties (downshifting and upconversion emission) and laser induced heating effect. *J. Phys. D: Appl. Phys.* **2017**, *50*, No. 045602.

DOI: 10.1021/acsomega.8b03606
ACS Omega 2019, 4, 6903−6913